

Decentralized Cooperation of Natural Gas and Power Systems with Preserved Privacy and Decision-Making Independence

Ahmad Nikoobakht^{1*}, Jamshid Aghaei², Gonçalo Pinto Mendes², Vahid Vahidinasab³

¹ Higher Education Center of Eghlid, Eghlid, Iran

² School of Energy Systems, Lappeenranta–Lahti University of Technology (LUT), Lappeenranta, Finland

³ Department of Engineering, School of Science and Technology, Nottingham Trent University, Nottingham, UK

*Corresponding Author: A. Nikoobakht (email: a.nikoobakht@eghlid.ac.ir)

Abstract: Modern power systems are likely to suffer from cascading contingencies, which pose multiple challenges to operators. In the event of such contingencies, power system operators must implement corrective actions, which could either be load curtailment or fast-ramping of generation assets, such as natural gas-fired units. Nevertheless, increased utilization of these units makes the power system vulnerable to gas pressure loss and interruption in the natural gas supply. Thus, it is essential to deliberate on the security constraints of natural gas networks in the operation of power systems. Nevertheless, the state-of-the-art energy flow models, applicable to both power and gas energy systems, are incapable of handling the complex relations between cascading contingencies and pipeline gas pressure loss. This study investigates an alternative approach that incorporates a novel AC power flow model and a dynamic gas flow model to treat these energy system interactions in an interoperable and simultaneous manner. Furthermore, electricity and natural gas system operators are independent of one another, which allows information privacy to be maintained. Using a hierarchical iterative algorithm covering both energy systems, the decentralized decision-making outlined in this paper ensures that only a very limited amount of information can be shared between the power system and the natural gas system operators, thus ensuring privacy. Finally, the numerical simulation is carried out on modified IEEE 30-bus electricity and 10-node gas systems and also on a larger test system of the IEEE 118-bus electricity and 10-node gas systems to demonstrate the efficiency of the proposed framework and the adopted decentralized approach.

Keywords: Cascading contingencies, network operators, power systems, natural gas system, security constraints, privacy

1. Introduction

Cascading contingencies are customary events in modern power systems (PS) that pose myriad challenges to PS operators. When confronted with such events, PS operators are forced to implement corrective actions, which could either be the curtailment of certain loads or the summoning of fast-ramping generation assets, such as natural gas-fired units (GFUs). Adopting the former is technically straightforward, but not economically attractive, whereas adopting the latter is, making it the most desirable option for PS operators. It must be noted, however, that GFUs are large natural gas clients, representing a substantial share of the demand in the gas networks, and that their recurring commitment and dispatch also pose challenges to natural gas system (NGS) operators. For instance, feeding GFUs with natural gas during peak-load hours can cause a pressure drop in gas pipelines, creating a shortage of supply to residential clients [1, 2].

The main proposed solution for ameliorating the risk of pressure drops in NGSs, while maintaining acceptable PS security levels in the occurrence of cascading contingencies, is to implement accurate security constraint models of natural gas flows to be managed by PS operators. However, the dynamic abilities of state-of-the-art models are limited. While the velocity of the gas flow in pipelines is lower than that of the electrical power flow in transmission lines, natural gas can be easily stored, according to its compressibility properties. Dynamic gas flow models should take this often overlooked, yet valuable feature into consideration by considering longer time period responses to the evolving demand and its potential disturbances. Such an approach could facilitate the security of the NGSs by allowing more commitment and dispatch of GFUs by PS operators under contingency circumstances. Therefore, it is crucial to consider security constraints and dynamic approximations of pipeline gas flow in collaborative operations of the PS and the NGS.

Analogous to pipeline gas flows in the NGS, power flows in the PS also require precise physical-laws-based modeling. Most research in the area of PS operation has focused on DC power flow models, rather than on AC models [3, 4]. However, the option of using DC power flow equations may result in computational inaccuracies, because a DC power flow model ignores reactive power and voltage magnitude [4]. Providing sufficient reactive power support and preserving voltage security are critical issues in PS operation. Furthermore, to achieve better modeling of the network conditions, the use of AC power flow models is even more important when the possibility of cascading contingencies in stressed power systems is being considered [4].

Recent years have seen an increased interest in developing convex relaxation methods to solve AC power flow models in power distribution and transmission systems. In [5], a second-order conic formulation has been proposed for AC power flow modeling in a distribution system [6]. In [7], a max–min optimization model for

identifying the worst contingencies has been developed for the security-constrained optimal power flow problem second-order cone problem. In [8], a conic form of this problem has been formulated, considering control devices, such as unified power flow controllers and phase-shifting and tap-changing transformers. Therefore, in this paper, a modified convexified AC power flow model based on a second-order conic relaxation method is developed.

The above discussion recognizes the importance of dynamic treatment of gas flows in the NGS, as well as that of accurate AC power flow modeling in the PS but does not address the interdependence of the two from the standpoint of an operator. The structure of an energy system involves dedicated operators of the PS and the NGS, each following specific market guidelines and regulations. A possible collaborative approach, however, involves the existence of a third operator actor, or “a unified operator,” who is responsible for managing the joint operations of the PS and the NGS. These coordinated operations require the collection of data to take place in centralized control facilities, which poses substantial challenges to the gathering and processing of information.

Based on the available literature in the area of PS-NGS cooperation, the main research and knowledge gaps are as follows:

- There has been increasing research interest in the topic of PS–NGS cooperation, partly owing to the many emerging interfaces between the PS and the NGS [2, 9-12]. In [2] and [9], an optimal DC power flow model is proposed within an integrated framework. In [10], a co-optimization model is proposed for the coordination of PS and NGS operators under continuous and discrete uncertainties. In [11], the impacts of fluctuating natural gas flows are studied for a short-term DC security-constrained unit commitment problem. In [12], a decentralized operation of multiarea electricity and natural gas transmission system is presented while considering wind energy and power-to-gas (P2G) technologies by decomposing a centralized problem into a set of computationally efficient subproblems to be solved independently for each area. Lastly, in [13], an AC power flow model is used for performing optimal day-ahead scheduling of electricity and gas system operations by minimizing the operational costs of the distribution system and the gas demand. All these studies share the view under which a unified system operator takes key decisions pertaining to both energy systems. However, the implied centralized operation methods cannot preserve data privacy for each energy system, nor can they enforce weighty investments on high-bandwidth communication links for exchanging data between operators. To cover this research gap, the present paper proposes a decentralized, three-level hierarchical solution method for the collaborative cooperation of the PS and the NGS that can preserve both the information privacy and the independence of decision-making for each energy system operator.

- Furthermore, cascading contingencies need to be considered in an environment of cooperation between the PS and the NGS. There is a considerable body of literature around the topic of cascade contingencies, but generally, these studies pertain to day-ahead scheduling of PS operations. For example, in [14], a trilevel optimization has been developed for energy and reserve scheduling in PS operation subject to the $n-k$ security criteria. The effect of multiple contingencies in PS operation [15] and planning [16, 17] has also been studied. In addition, in [10], a method has been presented to identify worst-case contingencies and wind uncertainty in a security-constrained unit commitment problem. Noticeably, none of the above studies uses AC power flow modeling, and all of them ignore the effect of worst-case scenario contingencies in the NGS. To fill in this gap, the current paper advances an adjustable robust AC constrained approach to identify multiple contingencies in the collaborative operation of the PS and the NGS. The proposed uncertainty modeling approach allows identifying the combination of the worst k -contingent scenario for the PS operator and investigates the impact of multiple contingencies on the gas flow and pressure in the NGS.

Accordingly, based on the above-mentioned research gaps, the main contributions of this paper are:

- (i) Implementation of a bi-level mixed-integer second-order conic model to represent AC power flows in transmission lines, as well as a gas network dynamic model to represent gas flow transients in pipelines;
- (ii) Development of a decentralized three-level hierarchical solution method for the collaborative operation of the PS and the NGS—in the proposed method, each operator acts under its own regulations and cooperates by periodically sharing a limited set of information. Therefore, the independence of decision-making and data privacy of each energy system operator is preserved.
- (iii) Development of a new adjustable robust AC contingency-constrained power flow to identify worst-case multiple contingencies in the collaborative operation of the PS and the NGS.

2. Problem formulation

2.1. Assumptions

The main assumptions of the proposed model are:

- All the contingencies in the PS are cascading contingencies;
- The cascade contingencies correspond to randomized outages in transmission lines;
- The gas compressor factor and the gas temperature are considered to be constant.

The formulation of the collaborative operation of the PS and the NGS with the robust second-order conic AC contingency-constrained approach is detailed in the following six subsections of this paper.

2.2. Objective function

The objective function (1) represents the total cost for the PS operator, i.e., Φ^E , and the NGS operator, i.e., Φ^G , respectively.

$$\Phi^{TC} = \min(\Phi^E + \Phi^G) \quad (1)$$

2.3. Convex and relaxed formulation of power system operation

The conventional AC power flow equations can be reformulated by only including quadratic and linear equations to circumvent nonlinear sinusoidal terms. The equations are convexified and relaxed under certain conditions.

The conic quadratic AC power flow formulation is given below:

$$\Phi^E = \sum_t \sum_n (c_n^G p_{nt}^G + c_n^{su} v_{nt} + c_n^{up} p_{nt}^u + c_n^{uq} q_{nt}^u) \quad (2)$$

$$v_{nt} - w_{nt} = u_{nt} - u_{n,t-1} \quad (3)$$

$$\sum_{t'=t}^{t-UT_n+1} u_{n,t'} \leq UT_n v_{nt} \quad (4)$$

$$\sum_{t'=t}^{t-DT_n+1} (1-u_{n,t'}) \leq DT_n w_{nt} \quad (5)$$

$$p_n^G u_{nt} \leq p_{nt}^G \leq \bar{p}_n^G u_{nt}, (\underline{\gamma}_n, \bar{\gamma}_n) \quad (6)$$

$$q_n^G u_{nt} \leq q_{nt}^G \leq \bar{q}_n^G u_{nt}, (\underline{\kappa}_n, \bar{\kappa}_n) \quad (7)$$

$$r_n u_{nt} \leq (p_{nt}^G - p_{n,t-1}^G) \leq \bar{r}_n u_{nt}, (\underline{\nu}_n, \bar{\nu}_n) \quad (8)$$

$$V_n^2 \leq e_{nt} \leq \bar{V}_n^2, (\underline{\chi}_n, \bar{\chi}_n) \quad (9)$$

$$0 \leq p_{nt}^U, \delta_{nt} \quad (10)$$

$$0 \leq q_{nt}^U, \eta_{nt} \quad (11)$$

$$p_{nt}^G + p_{nt}^U - p_{nt}^D = G_{nm} e_{nt} + \sum_{m=1, n \neq m} (G_{nm} c_{nm} + B_{nm} s_{nm}), \quad \mu_{nt} \quad (12)$$

$$q_{nt}^G + q_{nt}^U - q_{nt}^D = -B_{nm} e_{nt} - \sum_{m=1, n \neq m} (B_{nm} c_{nm} - G_{nm} s_{nm}), \quad v_{nt} \quad (13)$$

$$(-G_{nm} e_{nt} + G_{nm} c_{nm} + B_{nm} s_{nm})^2 + ((B_{nm} - b_{nm} / 2) e_{nt} - B_{nm} c_{nm} + G_{nm} s_{nm})^2 \leq \bar{f}_{nm}^2 \quad (14)$$

$$c_{nm}^2 + s_{nm}^2 = e_{nt} e_{mt} \quad (15)$$

$$\theta_{nt} - \theta_{mt} = \arctan(s_{nmt} / c_{nmt}) \quad (16)$$

Equation (2) represents the total power system operation cost. Note that the indices $\{t, n\}$ in (2) denote the time period (hour) and the electrical bus, respectively. The parameters $\{c_n^G, c_n^{su}, c_n^{up}, c_n^{uq}\}$ in Equation (2) denote the generation cost, the startup cost, and the cost of active and reactive load curtailment for the bus n , respectively. Further, the variables $\{p_{nt}^G, v_{nt}, p_{nt}^u, q_{nt}^u\}$ denote the active power generation of a generator unit, the binary variables related to a generator unit start-up, and the active and reactive unserved loads at the bus n , respectively. The electrical operation cost comprises four terms; the first and second terms show the unit generation cost and the unit startup cost, respectively, whereas the third and fourth terms show the unserved real and reactive power per bus, respectively. Note that the unserved real and reactive power per bus is considered in the proposed problem in order to avoid infeasibility. It is also pointed out that in normal operating conditions, the cost coefficients for the unserved loads are substantially higher than those for the generation costs. Equation (3) shows the conditions of the start-up and shutdown statuses of a generating unit (GU). In Equation (3), the variables $\{w_{nt}, u_{nt}\}$ denote binary variables related to the shutdown and status of a GU. The minimum on/off time for a GU is limited by Equations (4) and (5). In these equations, $\{UT_n, DT_n\}$ denote the minimum time for the on and off states of a GU. Equations (6) and (7) show the minimum and maximum limits of the real and reactive power generation of the GUs, respectively. In Equation (7), the variable q_{nt}^G shows the reactive power generation of a GU, and the parameters $\{\underline{p}_n^G / \bar{p}_n^G, \underline{q}_n^G / \bar{q}_n^G\}$ in Equations (6) and (7) represent the min/max active power generation and the min/max reactive power generation of a GU, respectively. The limits of the ramp-down/up rate of a GU are enforced by Equation (8). In this equation, the parameters $\underline{r}_n / \bar{r}_n$ indicate the ramp-down/up rate limits of a GU. The bus voltage magnitude is limited by Equation (9). The variable e_{nt} determines the voltage magnitude at the bus n . Further, the parameters $\underline{V}_n^2 / \bar{V}_n^2$ indicate the min/max quadratic voltage of an electrical bus. Equations (10) and (11) ensure that the unserved real and reactive power generation maintains positive values. In Equations (10) and (11), the variables p_{nt}^U / q_{nt}^U denote the active/reactive unserved load. Equations (12) and (13) are the active and reactive nodal balance equations for the electric network. Note that the index m is for an electrical bus. The parameters p_m^D / q_m^D denote the forecasted active/reactive load, and the variables c_{nmt} / s_{nmt} are auxiliary variables to define the term $V_{nt} V_{mt} \cos \theta_{nmt} / V_{nt} V_{mt} \sin \theta_{nmt}$. Moreover, the parameters $\{G_{nm} / B_{nm}, G_{nm} / B_{nm}\}$ are the real/imaginary part of the bus nm and the real/imaginary part of the line admittance nm , respectively.

Importantly, $\{\underline{\gamma}_{nt} / \bar{\gamma}_{nt}, \underline{\kappa}_{nt} / \bar{\kappa}_{nt}, \underline{v}_{nt} / \bar{v}_{nt}, \underline{\chi}_{nt} / \bar{\chi}_{nt}\}$ show the dual variables of Equations (6)–(9), respectively. In addition, $\{\delta_{nt}, \eta_{nt}, \mu_{nt}, \nu_{nt}\}$ relate to the dual variables of Equations (10)–(13), respectively.

The relationship between c_{nmt} , s_{nmt} and $e_{nt}e_{mt}$, the substituted variables pertaining to the *sin* and *cos* functions in the AC power flow equations [4] and [5], is imposed by Equations (14) and (16), which guarantees the consistency of the proposed model. In Equation (14), the parameter \bar{f}_{nm} is the maximum apparent power flow through a transmission line. Likewise, in Equation (16), the variable θ_{nt} denotes the voltage angle at a bus. Further details on the formulation of Equations (14)–(16) can be found in [4] and [5]. Equation (16), as a complementary constraint, is required for enforcing the AC power flow model into the PS operation problem. Note that the AC power flow model (14)–(16) is a nonconvex optimization problem that can be converted into a convex conic problem [18] by discarding Equation (16) and relaxing Equation (15), as in:

$$c_{nmt}^2 + s_{nmt}^2 \leq e_{nt}e_{mt} \quad (17)$$

The problem (2)–(14) and (17) is thus converted into a *convex conic optimization problem*. For the sake of having “well-behaved formulations,” Equations (14) and (17) have been replaced by equivalent equality and inequality equations, (18) to (26), as follows:

$$p_{nmt}^F = -G_{nm}e_{nt} + G_{nm}c_{nmt} + B_{nm}s_{nmt} \quad (18)$$

$$q_{nmt}^F = (B_{nm} - b_{nm}/2)e_{nt} - B_{nm}c_{nmt} + G_{nm}s_{nmt}, \psi_{nmt} \quad (19)$$

$$S_{nm}^F = \bar{f}_{nm}, \zeta_{nm} \quad (20)$$

$$\left(p_{nmt}^F\right)^2 + \left(q_{nmt}^F\right)^2 \leq \left(S_{nm}^F\right)^2 \quad (21)$$

$$D_{nmt}^1 = 2c_{nmt}, \alpha_{nm,t} \quad (22)$$

$$D_{nmt}^2 = 2s_{nmt}, \beta_{nm,t} \quad (23)$$

$$D_{nmt}^3 = e_n - e_m, \phi_{nm,t} \quad (24)$$

$$D_{nmt}^4 = e_{nt} + e_{mt}, \varphi_{nm,t} \quad (25)$$

$$\left(D_{nmt}^1\right)^2 + \left(D_{nmt}^2\right)^2 + \left(D_{nmt}^3\right)^2 \leq \left(D_{nmt}^4\right)^2 \quad (26)$$

It is pointed out that the variables p_{nmt}^F / q_{nmt}^F in Equations (18)/(19) are the active/reactive power flow of a transmission line, and the parameter S_{nm}^F in Equation (20) is the maximum apparent power flow through a transmission line. Further, the variables $\{D_{nmt}^1, D_{nmt}^2, D_{nmt}^3, D_{nmt}^4\}$ in Equations (22)–(25), are auxiliary variables

to model a conic AC power flow. Finally, $\{\psi_{nm,t}, \zeta_{nm}, \alpha_{nm,t}, \beta_{nm,t}, \phi_{nm,t}, \varphi_{nm,t}\}$ are dual variables for Equations (19)–(20) and (22)–(25), respectively.

2.4. Problem formulation of NGS operation

The NGS operation problem has similarities to the PS operation problem; natural gas flows from the gas supply to the customers through gas pipelines in the same way as electricity travels from the generation points to the electrical sinks across transmission and distribution lines. The mathematical equations describing the NGS are as follows:

$$\Phi^N = \sum_t \sum_i \left(C_i^{GG} G_{it}^W + C_i^{GS} (S_{it}^{in} + S_{it}^{out}) + C_i^{GU} \Gamma_{\omega, it}^U \right) \quad (27)$$

$$\frac{\partial \pi_{it}}{\partial t} = -K_1 \frac{\partial G_{ij,t}^F}{\partial x} \quad (28)$$

$$\frac{\partial \pi_{it}^2}{\partial x} = -K_2 (G_{ij,t}^F)^2 \quad (29)$$

$$\underline{\pi}_i \leq \pi_{it} \leq \bar{\pi}_i \quad (30)$$

$$\underline{G}_i^W \leq G_{it}^W \leq \bar{G}_i^W \quad (31)$$

$$L_{it} = L_{it}^E + L_{it}^N - \Gamma_{it}^U \quad (32)$$

$$0 \leq \Gamma_{it}^U \quad (33)$$

$$0 \leq G_{ijt}^F \quad (34)$$

$$\pi_{it} \leq \Lambda_c \pi_{jt} \quad (35)$$

$$E_{it} - E_{i,t-1} = S_{it}^{in} - S_{it}^{out} \quad (36)$$

$$\underline{E}_i \leq E_{it} \leq \bar{E}_i \quad (37)$$

$$\underline{S}_i^{in} \mathcal{G}_{it}^{in} \leq S_{it}^{in} \leq \bar{S}_i^{in} \mathcal{G}_{it}^{in} \quad (38)$$

$$\underline{S}_i^{out} \mathcal{G}_{it}^{out} \leq S_{it}^{out} \leq \bar{S}_i^{out} \mathcal{G}_{it}^{out} \quad (39)$$

$$\mathcal{G}_{it}^{in} + \mathcal{G}_{it}^{out} \leq 1 \quad (40)$$

$$L_{it}^e = A_{1,n} + A_{2,n} \bar{p}_{nt}^G + A_{3,n} (\bar{p}_{nt}^G)^2 \quad (41)$$

$$\sum_{i \in \mathcal{I}(t)} (S_{it}^{in} - S_{it}^{out}) + \sum_{p(i,j)} G_{ijt}^F - \sum_{p(j,i)} G_{jit}^F + \sum_{i \in \mathcal{G}(t)} G_{it}^W = L_{it} \quad (42)$$

$$p_{nt}^G = \bar{p}_{nt}^G \quad (43)$$

Similar to Equation (2), Equation (27) shows the total operation cost of the NGS problem, i.e., Φ^N , which includes the cost of gas production from natural gas wells (first term), i.e., $C_i^{GG} G_{it}^W$, the cost of gas inflow/outflow to/from a gas storage unit (GSU) (second term), i.e., $C_i^{GS} (S_{it}^{in} + S_{it}^{out})$, and the cost of unserved gas loads per node (third term), i.e., $C_i^{GU} \Gamma_{\omega,it}^U$. Here, the indices $\{i, j\}$ indicate gas nodes. Furthermore, in Equation (27), the parameters $\{C_i^{GG}, C_i^{GS}, C_i^{GU}\}$ are the production cost of a gas well, the gas storage cost for a gas storage unit (GSU), and the cost of an unserved gas load, respectively. In Equation (27), the variables $\{G_{it}^W, S_{it}^{in} / S_{it}^{out}, \Gamma_{\omega,it}^U\}$ denote the production of a gas well, the input/output gas to/from a gas storage unit, and the unserved gas load, respectively. Note that the gas flow through a gas pipeline follows Newton's second law and the law of the conservation of mass. This is described by Equations (28) and (29) for ideal conditions, i.e., while considering constant values for the gas compressor factor and the gas temperature. In these equations, π_{it} and $G_{ij,t}^F$ represent the node gas pressure and the gas flow rate at the location x and time t , respectively, under standard conditions. In Equations (28) and (29), K_1 and K_2 are constant parameters pertaining to the properties of the gas pipelines [12]. The limits on the gas pressure at a node are expressed by Equation (30). The parameters $\underline{\pi}_i / \bar{\pi}_i$ are the min/max gas pressure limits for the gas node i . The output of a natural gas well is constrained by Equation (31). In this equation, the parameters $\underline{G}_i^W / \bar{G}_i^W$ are the min/max gas production for a gas well. Equation (32) gives the total gas load (L_{it}) for the electric consumption (L_{it}^E), the residential load (L_{oit}^R), and the unserved gas load ($\Gamma_{\omega,it}^U$). Equations (33) and (34) ensure that the unserved gas load and the gas flow direction remain positive, respectively. Terminal nodal pressures in the gas pipeline related to gas compressors are constrained through a compressor factor indicated in Equation (35). A constant factor for a gas compressor in this equation is denoted by Λ_c . The operation mode of the gas storage in a GSU is represented by Equation (36). In this equation, the variable E_{it} is the volume of gas stored in the GSU i . The limitations on the stored gas capacity, gas inflow, and gas outflow for a GSU are described through Equations (37)–(39). In these equations, the parameters $\{\underline{E}_i / \bar{E}_i, \underline{S}_i^{in} / \bar{S}_i^{in}, \underline{S}_i^{out} / \bar{S}_i^{out}\}$ are the min/max gas stored in a GSU, the min/max gas input limit, and the min/max gas output limit from a GSU, respectively. Additionally, $\mathcal{G}_{it}^{in} / \mathcal{G}_{it}^{out}$ are binary variables stating the input/output modes of a GSU. The statuses of the gas inflow or the gas outflow for a GSU are specified in Equation (40). The

GFU's link to the PS is perceived as a main industrial load for NGS operators. The natural gas consumption of the GFUs is represented in Equation (41). In this equation, the variable \bar{p}_m^G shows the power generation of a GFU, and the parameters $\{A_{1,n}, A_{2,n}, A_{3,n}\}$ show the fuel coefficients of a GFU. The summation of the gas outflows and inflows from a gas node is equal to zero, which is shown by Equation (42). As mentioned above, the GFUs connected to the PS are formulated as a gas load on the NGS side and as a boundary source bus on the PS side. Specifically, in Equation (43), \bar{p}_m^G represents the boundary load in the NGS, whereas p_m^G represents the generation source in the PS.

2.5. Implicit finite difference approximation

It is hard to handle Equations (28) and (29) by using analytical methods. As an alternative to analytical methods, numerical methods that discretize the functions can evaluate the dependent variables at discrete points in a span of time and space. In this study, the Euler finite difference numerical method is used to approximate Equations (28) and (29), by substituting derivative terms with equivalent difference quotients [19]. Thus, Equations (28) and (29) can be converted into a set of algebraic equations, i.e., Equations (44) and (45), at (i, t) with the time step Δt and the spatial step Δx :

$$\frac{\pi_{i,t} - \pi_{i,t-1}}{\Delta t} = \frac{K_1}{2\Delta x_{ij}} (G_{ijt}^F - G_{jit}^F) \quad (44)$$

$$\frac{\pi_{i,t}^2 - \pi_{j,t}^2}{\Delta t} = \frac{K_2}{2\Delta x_{ij}} G_{ij,t}^2 \quad (45)$$

Note that in Equations (44) and (45), increasing the number of time steps Δt and spatial steps Δx can improve the accuracy of the numerical computation, albeit at the expense of a higher computational burden.

2.6. Contingency selection mechanism

In its original form, the security-constrained cooperation of the PS and the NGS is a deterministic or a stochastic problem, wherein the number of contingencies is prespecified. Nevertheless, in the cooperation problem proposed in this paper, the PS operator selects the cascading contingencies, including k outages, based on a *max-min* optimization formulation. The *max-min* formulation is a bi-level problem wherein the upper-level problem maximizes the post-contingency total cost, including thermal generation cost, start-up cost, and active and reactive load shedding cost, in order to select the contingency or contingencies, whereas the lower-level problem performs optimal *corrective actions* over the selected contingency or contingencies in the upper-level problem. This bi-

level formulation is explained as follows:

$$\Phi^W = \max_{\sigma \in \Omega} \min_{p \in P(\sigma)} \sum_t \sum_n (c_n^u p_{nt}^G + c_n^{up} p_{nt}^U + c_n^{uq} q_{nt}^U) \quad (46)$$

$$\Omega = \left\{ \sum_{l \in L} (1 - \sigma_{nm}) \leq k, \forall \sigma_{nm} \in \{0, 1\} \right\} \quad (47)$$

$$P(\sigma) = \{p: (6) - (7), (9)\} \quad (48)$$

$$p_{nt}^G + p_{nt}^U - p_{nt}^D = \sum_{m=1, n \neq m} p_{nm,t}^F \quad (49)$$

$$q_{nt}^G + q_{nt}^U - q_{nt}^D = \sum_{m=1, n \neq m} q_{nm,t}^F \quad (50)$$

$$p_{nm,t}^F = (-G_{nm} p_{nt}^G + G_{nm} p_{nm,t}^G + B_{nm} q_{nm,t}^F) \sigma_{nm}, \quad \xi_{nm,t} \quad (51)$$

$$q_{nm,t}^F = ((B_{nm} - b_{nm}/2) p_{nt}^G - B_{nm} p_{nm,t}^G + G_{nm} q_{nm,t}^F) \sigma_{nm}, \quad \psi_{nm} \quad (52)$$

$$R_n^D \leq p_{nt}^G - p_{nt}^U \leq R_n^U, (\underline{\lambda}_{nt}, \bar{\lambda}_{nt}) \quad (53)$$

$$(17) - (26), \forall \mathfrak{A} \quad (54)$$

The *max–min* objective function (46) is similar to Equation (1). In Equation (46), the variable Φ^W shows the total operation cost post-contingency state. The feasibility region of the upper-level problem, i.e., Ω , is defined by Equation (47). It is worth remembering here that all the variables include the superscripts \mathfrak{A} referring to the post-contingency state. Note that the status of the transmission line nm in the *max–min* formulation is represented by the binary variable σ_{nm} , where $\sigma_{nm} = 1$ or $\sigma_{nm} = 0$ indicates if the line is in service or out of service, respectively. The maximum number of contingencies is restricted by Equation (47) with the inclusion of the parameter k . Similarly, p_{nt}^G in Equation (48) denotes the lower-level problem variables, which are limited by the lower-level problem equations $P(\sigma)$. Equation (48) includes Equations (6)–(7) and (9), which are described in detail above. Equations (49) and (50) are similar to Equations (12) and (13), and they are the active and reactive nodal balance equations in the contingency condition. Equations (51) and (52) are identical to Equations (18) and (19) while comprising the binary variable σ_{nm} in the active and reactive power flow terms. Note that $\xi_{nm,t}$ is the dual variable for Equation (51). If $\sigma_{nm} = 1$, Equations (51) and (52) are considered the AC power flow equations, else, the active and reactive power flows of a transmission line nm are enforced to zero, which indicates that the line is open or out of service. To formulate a standard corrective action for the PS operation problem between the normal

and the contingent states, the ramping-up/down variations of a GU are restricted by Equation (53). The parameters R_n^D / R_n^U indicate the ramp-down/ramp-up rate limits of a unit in the contingent state. Furthermore, $\{\underline{\lambda}_n, \bar{\lambda}_n\}$ show the dual variables for Equation (53). Equation (54) includes Equations (17)–(26), which are described in detail above.

2.7. Corrective action modeling

When cascading contingencies are identified by the proposed *max–min* problem (46)–(54), the standard corrective action for a PS operator is performed. Note that the corrective action operation problem guarantees that as a result of a cascading contingency, the power generation of GUs is changed within a confidence range to satisfy the PS operation constraints. The corrective action formulation is as follows:

$$\min \Phi^E = \sum_t \sum_n (c_n^G p_{nt}^G + c_n^{su} v_{nt} + c_n^u p_{nt}^u + c_n^u q_{nt}^u) + \sum_t \sum_n (c_n^u p_{nt}^{G\%} + c_n^{up} p_{nt}^{U\%} + c_n^{uq} q_{nt}^{U\%}) \quad (55)$$

Pre-contingency constraints:

$$(2)–(13) \& (18)–(26) \quad (56)$$

Post-contingency constraints

$$(49)–(54), \forall \% \quad (57)$$

The objective function (55) represents the PS operating cost under the pre- and all post-contingency states. The variable Φ^E shows the electrical operation cost for the pre/post-contingency states. The corrective action problem, i.e., Equations (56) and (57), considers two sets of constraints to satisfy both the pre/post-contingency operating states. Note that Equation (56) includes Equations (2)–(13) and (18)–(26), and Equation (57) comprises Equations (49)–(54), which are described in detail above. Moreover, Equations (49)–(54) include post-contingency variables, which have superscripts $\%$. In addition, the pre/post-contingency variables in the corrective action problem should be changed so that they concurrently guarantee both the pre/post-contingency constraints.

2.8. Collaboration between electricity and natural gas systems

In the proposed scheme, each system is controlled by its own independent operator, which cooperates with other interconnected systems by sharing a limited set of data to minimize the total operation cost of each system. An overview of the coordination scheme for the PS and NGS operators in both centralized and decentralized decision-making strategies is shown on the left and right sides of Fig. 1, respectively. In Fig. 1, it is assumed that the positive direction of the energy exchange is from the NGS to the PS. Thus, the GFUs are modeled as loads for the NGS operator and the generator for the PS operator.

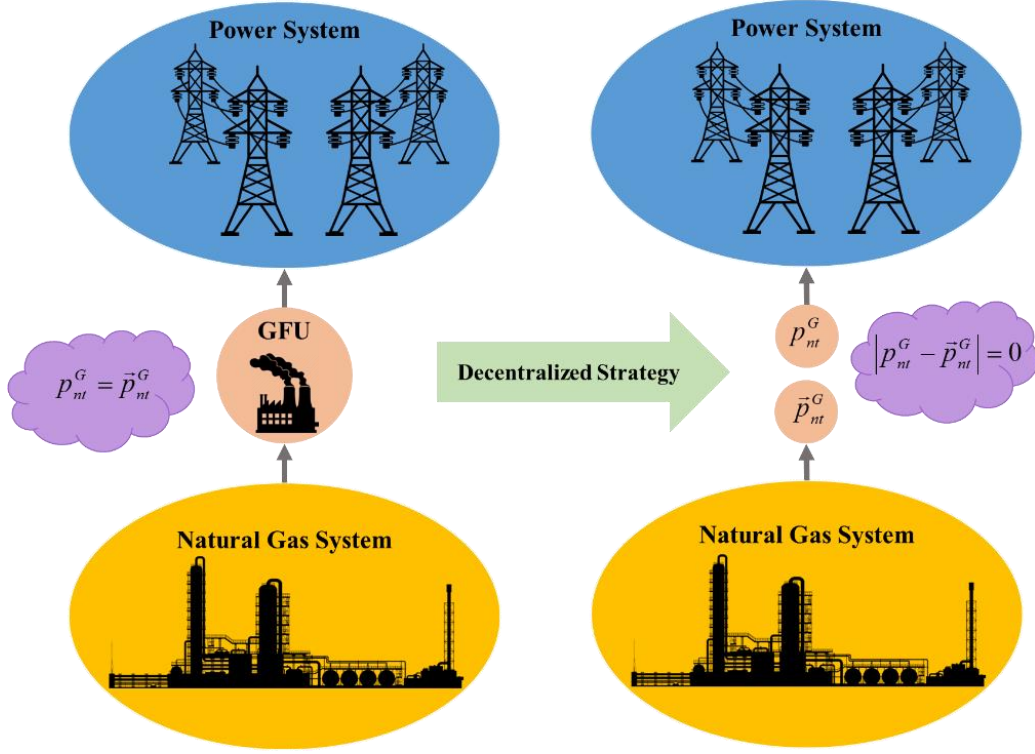


Fig. 1. Information shared between the PS and NGS operators.

The consistency constraint, i.e. $p_{nt}^G = \bar{p}_{nt}^G$, is considered in the centralized decision-making strategy, and both systems keep track of both assets and try to minimize total operational costs, whereas the consistency constraint is relaxed in the decentralized decision-making strategy. In other words, in the decentralized decision-making strategy, the inner topological data and the operation information including electric power generation, natural gas production, energy conversion, and the physical and technical characteristics of both the PS and the NGS are kept confidential for each system operator. Accordingly, only the generation states of the natural gas-fired units (GFUs) are shared among the PS and NGS operators in the coordination process for preserving the decision-making independence and information privacy of an individual system. For example, in the decentralized decision-making strategy, proprietary system information is not displayed for any system in Fig. 1, and thus, each system is simply represented by an ellipsoid region. The right side of Fig. 1 shows a fully decentralized operation, and the collaboration between both systems is addressed by shared information. On the right side of Fig. 1, two variables including the target variables $\{p_{nt}^G\} \in ta$ and the response variables $\{\bar{p}_{nt}^G\} \in re$ are introduced in the decentralized model, which highlights the shared information. In fact, on the right side of Fig. 1, the power generation of the GFU, i.e., p_{nt}^G , measured by the PS operator, is defined as the target variable, and the variable \bar{p}_{nt}^G , determined by the NGS operation, is defined as the response variable. Note that the variable \bar{p}_{nt}^G can be converted into a

natural gas load for the NGS operator by using Equation (41). It is also noteworthy that in the decentralized operation, the consistency constraint $|ta - re| = 0$ must be satisfied.

3. Solution Methodology

Here, an effective decentralized solution method based on a three-level hierarchical approach is proposed to solve the robust AC contingency-constrained collaborative operation of the PS and the NGS. Accordingly, the proposed solution approach comprises three levels:

- The first level is related to the corrective action security-constrained PS operation problem, which minimizes the electrical generation costs for both the pre/post-contingency operating conditions;
- The second level is related to the NGS operation while minimizing the gas production costs,
- The third level pertains to identifying cascading contingencies, based on the mixed-integer conic maximization problem.

The following subsections explain the proposed three-level hierarchical solution method in detail.

3.1. The first and second levels

As mentioned above, in the real world, the collaborative operation of the PS and the NGS under one operator is unrealistic, because both systems have independent operators and face substantially different regulations, although preserving data privacy is also of critical concern. Furthermore, GFUs are simultaneously power generators in the PS and consuming loads in the NGS, which supports the need for a decentralized approach in the potential collaboration between operators. Accordingly, the proposed solution method decomposes the problem of collaborative operation between the PS and NGS operators into two independent operation problems. In summary, in this independent bi-level decentralized hierarchical method, the PS operation problem, i.e., Equations (55)–(57), and the NGS operation problem, i.e., Equations (27)–(42), are treated as first and second levels, respectively. Thus, the PS and NGS operators are operated individually. The data transactions between the PS and NGS operation problems can be attained with a target variable, i.e., $ta = \{P_m^G\}$, and a response variable, i.e., $re = \{\bar{p}_m^G\}$, in the PS and NGS operation problems, respectively. The fully decentralized optimization is converged when the target and response variables converge to a same value. The following subsections explain the formulations of the decentralized collaborative operation of both energy systems.

The first level (corrective action of PS operation): The formulation of corrective actions in the PS operation problem takes the following shape:

$$\min \Phi^E + \tau \left((p_{nt}^G)^v - (\bar{p}_{nt}^G)^{(v-1)} \right) + \bar{\tau} \left\| (p_{nt}^G)^v - (\bar{p}_{nt}^G)^{(v-1)} \right\|_2^2 \quad (58)$$

$$(56) - (57) \quad (59)$$

The first term of the objective function (58) is the same as Equation (55). The penalty function consists of two main terms, the linear $\tau \left((p_{nt}^G)^v - (\bar{p}_{nt}^G)^{(v-1)} \right)$ and the quadratic $\bar{\tau} \left\| (p_{nt}^G)^v - (\bar{p}_{nt}^G)^{(v-1)} \right\|_2^2$. The parameters τ and $\bar{\tau}$ are multipliers associated with the linear and quadratic terms, respectively, and they will be updated during the iterative solution process. An important feature of the second-order penalty function is that it is a convex quadratic curve. The convex quadratic term in Equation (58) is nonlinear, but it can be linearized as given by [20].

The penalty function includes the target and response variables, i.e., p_{nt}^G and \bar{p}_{nt}^G , which should be prespecified as per the agreement between the PS and NGS operators. Thus, the target variable p_{nt}^G is specified by the PS operation problem, while the response variable value \bar{p}_{nt}^G is determined by the NGS operation problem because the equality coupling constraints of Equation (43) should be satisfied. Note that \bar{p}_{nt}^G , in Equation (58), is a constant value determined by the NGS operation problem. The convex quadratic term in Equation (58) is nonlinear, but it can be linearized as given by [20]. Equation (59) includes Equations (56)–(57), which are described in detail above.

The second level (NGS operation): The formulation of the NGS operation problem can be presented as:

$$\text{Min } \Phi^N + \tau \left((\bar{p}_{nt}^G)^v - (\hat{p}_{nt}^G)^{(v-1)} \right) + \bar{\tau} \left\| (\bar{p}_{nt}^G)^v - (\hat{p}_{nt}^G)^{(v-1)} \right\|_2^2 \quad (60)$$

$$(27), (30) - (42) \text{ and } (44) - (45) \quad (61)$$

As in Equation (58), the first term of the objective function (60) is the total production cost of the NGS operation problem, i.e., Equation (27). In addition, the second term is explained above for Equation (58). Similar to Equation (58), the second term in (60) is a penalty function. This function includes the target and response variables, the target variable \bar{p}_{nt}^G is determined by the PS operation problem, and the response variable \hat{p}_{nt}^G is determined by the NGS operation problem. Note that, as in Equation (60), the variable \hat{p}_{nt}^G is a constant value.

Finally, Equation (61) includes Equations (27), (30)–(42) and (44)–(45), which are described in detail above.

Convergence mechanism for the first and second levels: The target and response variables, i.e., p_{nt}^G and \mathbf{p}_{nt}^G , are exchanged between the PS and NGS operation problems through an iterative process until constraints (62) and (63) are satisfied (stop criteria).

$$\begin{cases} \left| \left(p_{nt}^G \right)^v - \left(p_{nt}^G \right)^{(v-1)} \right| \leq \varepsilon \\ \left| \left(\mathbf{p}_{nt}^G \right)^v - \left(\mathbf{p}_{nt}^G \right)^{(v-1)} \right| \leq \varepsilon \end{cases} \quad (62)$$

$$\left| \left(p_{nt}^G \right)^v - \left(\mathbf{p}_{nt}^G \right)^v \right| \leq \varepsilon \quad (63)$$

In constraints (62) and (63), ε is the critical error level, and the subscript v shows the number of iterations between the PS and NGS operation problems.

3.2. The third level (Identifying worst-case contingencies)

As mentioned above, the problem of identifying the worst contingency or contingencies can be modeled as a *max–min* conic problem, i.e., Equations (46)–(54). However, it is intractable to solve directly the *max–min* conic problem (46)–(54) with standard commercial optimization packages. Accordingly, the lower-level conic problem (46)–(54) is transformed into its equal dual problem by means of conic relaxation duality theory [21]. When the binary variable \hat{u}_{nt} obtained from the first-level optimization is fixed in the lower-level problem, the problem becomes convex and conic, and can then be replaced by its dual. Thus, the *max–min* conic optimization model is converted into a *max–max* conic optimization model based on [22], [21] which is a mixed-integer single-level problem. The proposed formulation is as follows:

$$\max \sum_n \left(\begin{array}{l} \underline{p}_n^G \hat{u}_{nt} \gamma_{nt} + \bar{p}_n^G \hat{u}_{nt} \bar{\gamma}_{nt} + \underline{r}_n \hat{u}_{nt} \underline{\nu}_{nt} + \bar{r}_n \hat{u}_{nt} \bar{\nu}_{nt} + V_{-n}^2 \underline{\chi}_{nt} + \bar{V}_n^2 \bar{\chi}_{nt} \\ + p_{nt}^D \mu_{nt} + q_{nt}^D \nu_{nt} + (R_n^D + p_{nt}^{G0}) \bar{\lambda}_{nt} + (p_{nt}^{G0} - R_n^D) \underline{\lambda}_{nt} \end{array} \right) + \sum_{(n,m) \in L} \bar{f}_{nm} \zeta_{nm} \quad (64)$$

$$\sum_{l \in L} (1 - \sigma_{nm}) \leq k, \quad \forall \sigma_{nm} \in \{0,1\} \quad (65)$$

$$\underline{\gamma}_{nt} + \bar{\gamma}_{nt} + \underline{\nu}_{nt} + \bar{\nu}_{nt} + \underline{\nu}_{n,t-1} + \bar{\nu}_{n,t-1} + \mu_{nt} + \underline{\lambda}_{nt} + \bar{\lambda}_{nt} = C_n^G \quad (66)$$

$$\underline{\kappa}_{nt} + \bar{\kappa}_{nt} + \nu_{nt} = 0 \quad (67)$$

$$\delta_{nt} + \mu_{nt} = c_n^{up} \quad (68)$$

$$\nu_{nt} + \nu_{nt} = c_n^{uq} \quad (69)$$

$$\left(\begin{aligned} & \underline{\chi}_{nt} + \bar{\chi}_{nt} + \sum_{j=1, j \neq i} G_{nm} t_{nm,t}^1 - \sum_{j=1, j \neq i} (B_{nm} - b_{nm} / 2) \cdot t_{nm,t}^2 \\ & - \sum_{j=1, j \neq i} G_{nm} t_{nm,t}^3 + \sum_{j=1, j \neq i} (B_{nm} - b_{nm} / 2) \cdot t_{nm,t}^4 + \sum_{j=1, j \neq i} \phi_{nm,t} + \sum_{j=1, j \neq i} \varphi_{nm,t} \end{aligned} \right) \leq 0 \quad (70)$$

$$-G_{nm} t_{nm,t}^1 + B_{nm} t_{nm,t}^2 + G_{nm} t_{nm,t}^3 - B_{nm} t_{nm,t}^4 + 2\alpha_{nm,t} = 0 \quad (71)$$

$$-B_{nm} t_{nm,t}^1 - G_{nm} t_{nm,t}^2 + B_{nm} t_{nm,t}^3 + G_{nm} t_{nm,t}^4 + 2\beta_{nm,t} = 0 \quad (72)$$

$$t_{nm,t}^1 = \mu_{n,t} - h_{nm,t}^1 \quad (73)$$

$$\underline{\mu}_n \sigma_{nm} \leq t_{nm,t}^1 \leq \bar{\mu}_n \sigma_{nm} \quad (74)$$

$$\underline{\mu}_n (1 - \sigma_{nm}) \leq h_{nm,t}^1 \leq \bar{\mu}_n (1 - \sigma_{nm}) \quad (75)$$

$$t_{nm,t}^2 = \nu_{n,t} - h_{nm,t}^2 \quad (76)$$

$$\underline{\nu}_n \sigma_{nm,t} \leq t_{nm,t}^2 \leq \bar{\nu}_n \sigma_{nm,t} \quad (77)$$

$$\underline{\nu}_n (1 - \sigma_{nm,t}) \leq h_{nm,t}^2 \leq \bar{\nu}_n (1 - \sigma_{nm,t}) \quad (78)$$

$$t_{nm,t}^3 = \xi_{nm,t} - h_{nm,t}^3 \quad (79)$$

$$\underline{\xi}_{nm} \sigma_{nm,t} \leq t_{nm,t}^3 \leq \bar{\xi}_{nm} \sigma_{nm,t} \quad (80)$$

$$\underline{\xi}_{nm,t} (1 - \sigma_{nm,t}) \leq h_{nm,t}^3 \leq \bar{\xi}_{nm,t} (1 - \sigma_{nm,t}) \quad (81)$$

$$t_{nm,t}^4 = \psi_{nm,t} - h_{nm,t}^4 \quad (82)$$

$$\underline{\psi}_{nm} \sigma_{nm,t} \leq t_{nm,t}^4 \leq \bar{\psi}_{nm} \sigma_{nm,t} \quad (83)$$

$$\underline{\psi}_{nm} (1 - \sigma_{nm,t}) \leq h_{nm,t}^4 \leq \bar{\psi}_{nm} (1 - \sigma_{nm,t}) \quad (84)$$

$$\xi_{nm,t}^2 + \psi_{nm,t}^2 \leq \zeta_{nm,t}^2 \quad (85)$$

$$\alpha_{nm,t}^2 + \beta_{nm,t}^2 + \phi_{nm,t}^2 \leq \varphi_{nm,t}^2 \quad (86)$$

Equation (64) is the objective function of the mixed-integer AC security-constrained conic problem. Equation (65) is similar to Equation (47). Equations (66)–(69) are dual constraints related to the primal variables $p_{nt}^G, q_{nt}^G, p_{nt}^U$ and q_{nt}^U , respectively. $\{t_{nm,t}^{(\oplus)}, h_{nm,t}^{(\oplus)}\}$ are dual variables. Equations (70)–(86) are the nonlinear dual constraints. Nonlinearities originate from the product of a binary variable with a continuous one. These products can be linearized by using the method introduced in [22] and [23].

3.3. Summary of the solution process

The summary of the proposed three-level hierarchical method is given in Fig. 2. As can be seen in the figure, the proposed solution method has three levels/iteration loops, i.e., Loops I, II, and III. Accordingly, the solution procedure can be described in eight steps as follows:

Step 0: Initialize the values for $\left\{ \left(\begin{smallmatrix} \mathbf{r}^G \\ \hat{p}_m^G \end{smallmatrix} \right)^v, \tau^{(w)}, \bar{\tau}^{(w)} \right\}$ and set the iteration index $\{v, w, k\} = 0$, respectively, for

Loops I to III;

Step 1: Set $v \leftarrow v + 1$. Solve the first-level problem, i.e., Equation (58) subject to Equation (59), for the response variable $\left(\begin{smallmatrix} \mathbf{r}^G \\ \hat{p}_m^G \end{smallmatrix} \right)^{(v-1)}$, which is specified by the prior iteration in the second-level problem, to obtain the target variable $\left(p_m^G \right)^v$;

Step 2: Solve the NGS operation problem, i.e., Equation (60) subject to Equation (61), for the fixed target variable $\left(\hat{p}_m^G \right)^{(v-1)}$ to find the response variable $\left(p_m^G \right)^v$;

Step 3: Here, the convergence of Loop I, named LC-I, is checked by Equation (62). If Equation (62) is larger than the prespecified error level, go back to Step 1, for the next iteration, else, go to Step 4. Note that the parameters $\tau^{(w)}$ and $\bar{\tau}^{(w)}$ are constant values and are not updated in the Loop I process (only $\left\{ \left(p_m^G \right)^v, \left(\begin{smallmatrix} \mathbf{r}^G \\ \hat{p}_m^G \end{smallmatrix} \right)^v \right\}$ should be updated);

Step 4: Check the Loop II convergence (LC-II), i.e., constraint (63). Go to Step 5, if constraint (63) is not satisfied, else, the optimal results $\left\{ \left(p_m^G \right)^v, \left(\begin{smallmatrix} \mathbf{r}^G \\ \hat{p}_m^G \end{smallmatrix} \right)^v \right\}$ are attained; thus, go to Step 6.

Step 5: Update $w \leftarrow w + 1$ and the multiplier values, i.e., $\tau^{(w)}$ and $\bar{\tau}^{(w)}$ Equations (87) and (88):

$$\tau^{(w+1)} = \tau^{(w)} + 2 \left(\bar{\tau}^{(w)} \right)^2 \left(\left(p_m^G \right)^w - \left(\begin{smallmatrix} \mathbf{r}^G \\ \hat{p}_m^G \end{smallmatrix} \right)^w \right) \quad (87)$$

$$\bar{\tau}^{(w+1)} = \gamma \tau^{(w)} \quad (88)$$

In Equation (88), the value of γ should be chosen larger than 1 to speed up the solution time and obtain solution results. Further details about the updating process for the multiplier values of $\tau^{(w)}$ and $\bar{\tau}^{(w)}$ can be found in [24].

Step 6: Solve the third-level problem, i.e., Equation (64) subject to Equations (65)–(86), with the fixed values of \hat{u}_m obtained from the first-level problem to find the worst-case contingencies, i.e., σ_{mm} , and go to Step 7.

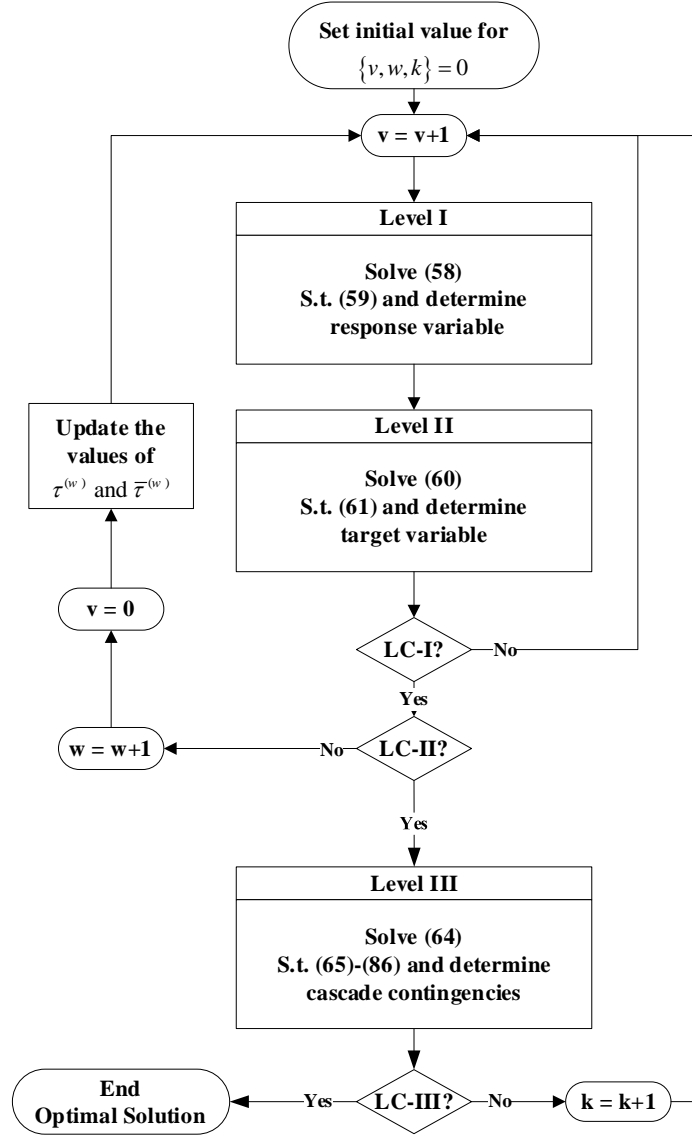


Fig. 2. Summary of the three-level hierarchical method.

Step 7: Check the convergence of Loop III, named LC-III, i.e., $|u_{nr}^k - u_{nr}^{(k-1)}| = 0$; if the convergences for LC-III are satisfied, the solution procedure is terminated and the current values of u_{nr}^k are returned as the optimal solution. Else, σ_{nm} will be added to the post-contingency constraints in the first-level problem. In addition, the iteration counter of Loop III, i.e., $k \leftarrow k + 1$, is updated; go to Step 1 for the following iteration for Loop III.

4. Case Studies

In this paper, a modified IEEE 30-bus transmission system with a ten-node NGS (which is named the IEEE-30 bus-10-node electrical–gas system) is implemented to evaluate the performance of the suggested decentralized collaborative operation of the PS and the NGS with the cascading contingencies state. The PS and NGS grids are

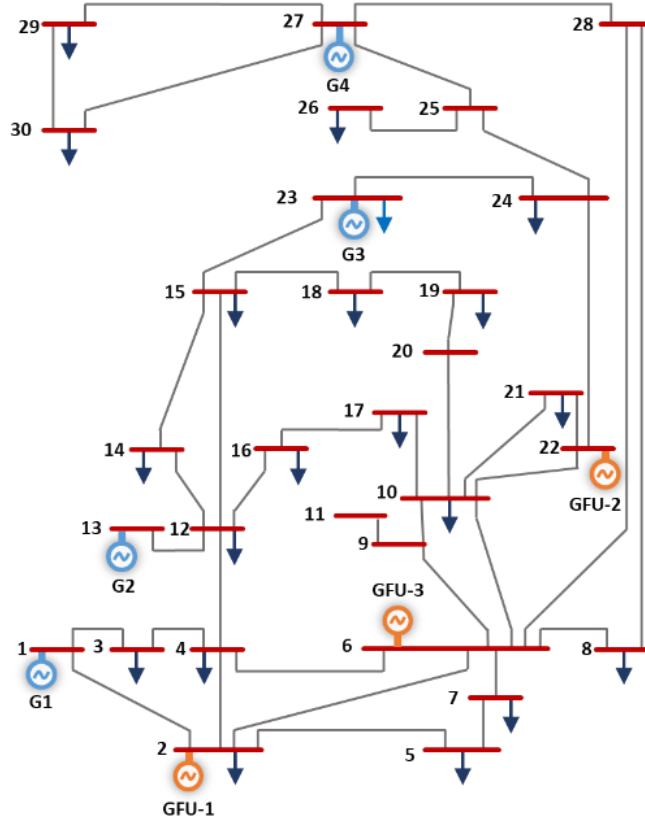


Fig.3: Modified IEEE 30-bus system with three GFUs.

illustrated in Figs. 3 and 4, respectively. As shown in Fig. 2, the power grid includes three GFUs (orange), four fossil-fueled units (blue), 20 loads, and 41 transmission lines. Further information about the loads, transmission lines, and fossil units is provided in [25]. The NGS in Fig. 4 has three gas wells, seven gas loads, and ten gas pipelines. More details about the GFUs and the gas transmission system parameters are given in the file “[Gas transsmion_118_10.xls](#)” in “[motor.ece.iit.edu/data](#)”. The peak gas load is 10,000 kcf. Additionally, the gas load and the electrical load at each hour, in per unit, are given in Fig. 5. Finally, the proposed optimization problem is carried out in a PC with 16 GB RAM and a CPU with eight processors clocking at 4.50 GHz. The optimization problem is programmed in the GAMS and solved by CPLEX (mixed-integer linear problem) and Gurobi 6.5 (mixed-integer second-order conic problem). To evaluate the performance of the proposed decentralized collaborative operation of the PS and NGS problem with the dynamic gas flow constraints (DGFCs) and the three-level hierarchical solution method, four case studies are considered.

4.1. Cooperation of the PS and the NGS with/without the DGFCs

The collaborative operation of the PS and the NGS with and without the dynamic gas flow constraints (DGFCs) is compared in Tables 1 and 3. These tables show that the electrical operation cost with the DGFCs is reduced for

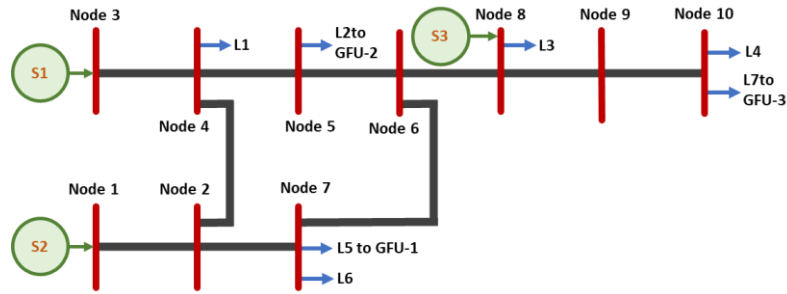


Fig. 4: Topology of the 10-node gas system.

each k and cooperation method. As expected, the gas operation costs with the DGFCs are increased, because the natural gas can be stored in gas pipelines. Once the DGFCs are considered by the proposed cooperation problem, the amount of daily natural gas consumption in the GFUs is supplied by the volume of natural gas that would be stored in the natural gas pipelines. In this condition, the total gas operation cost for the NGS is increased. Further, Tables 1, 2 and 3 show an overview of the electrical and gas unserved loads. It is apparent from these tables that the gas and electrical unserved loads are reduced for the DGFCs. These results are inevitable, because the NGS is preferentially operated to supply the high-priority (residential) natural gas loads, and supplying the GFU is in the lower-priority delivery contract service. Consequently, the contribution of GFUs to the power supply is reduced when the DGFCs are not considered in the proposed cooperation problem. Furthermore, the DGFCs provide a backup option once natural gas is not readily supplied to GFUs at gas peak hours. The results suggest that when the DGFCs are considered in the cooperation problem, the solution time is increased, owing to the consideration of more constraints. Nevertheless, implementing parallel processing and introducing other shortcuts in the mathematical methods can reduce the solution time.

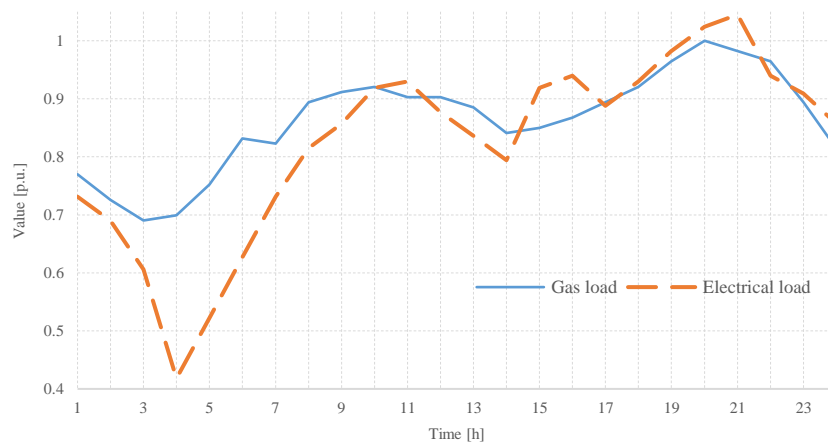


Fig. 5: Gas load and electrical load profiles in p.u.

Table 1: Comparison of operation results between different operation strategies; for $k = 0$; IEEE-30 bus-10-node electrical–gas system.

| Method | | Φ^E [k\$] | Φ^G [k\$] | Gas unserved load [kcf] | Electrical unserved load [MWh] | Time [min] |
|------------------|----|-------------------|-------------------|-------------------------------|--------------------------------------|---------------|
| Without DGFCs | DM | 67.3 | 87.4 | 21.1 | 0 | 4 |
| | CM | 67.2 | 87.2 | 20.2 | 0 | 2 |
| | IM | 68.1 | 85.6 | 60.3 | 0 | 2 |
| With DGFCs | DM | 66.8 | 88.1 | 15.1 | 0 | 8 |
| | CM | 66.7 | 88.0 | 15.1 | 0 | 5 |
| | IM | 67.8 | 85.4 | 59.3 | 0 | 5 |

Table 2: Comparison of operation results between different operation strategies; for $k = 1$; IEEE-30 bus-10-node electrical–gas system.

| Method | | Φ^E [k\$] | Φ^G [k\$] | Gas unserved load [kcf] | Electrical unserved load [MWh] | Time [min] |
|------------------|----|-------------------|-------------------|-------------------------------|--------------------------------------|---------------|
| Without DGFCs | DM | 71.5 | 96.5 | 33.3 | 0 | 6 |
| | CM | 71.3 | 96.3 | 32.1 | 0 | 3 |
| | IM | 74.1 | 89.6 | 69.2 | 10.3 | 3 |
| With DGFCs | DM | 69.3 | 98.4 | 25.1 | 0 | 10 |
| | CM | 69.3 | 98.2 | 24.1 | 0 | 7 |
| | IM | 74.1 | 89.4 | 68.8 | 8.6 | 7 |

Table 3: Comparison of operation results between different operation strategies; for $k = 2$; IEEE-30 bus-10-node electrical–gas system.

| Method | | Φ^E [k\$] | Φ^G [k\$] | Gas unserved load [kcf] | Electrical unserved load [MWh] | Time [min] |
|------------------|----|-------------------|-------------------|-------------------------------|--------------------------------------|---------------|
| Without DGFCs | DM | 92.5 | 122.1 | 41.1 | 5.2 | 9 |
| | CM | 92.4 | 122.0 | 39.2 | 5.1 | 6 |
| | IM | 106.1 | 90.4 | 99.2 | 13.3 | 6 |
| With DGFCs | DM | 91.9 | 123.1 | 34.2 | 3.2 | 11 |
| | CM | 91.9 | 123.1 | 34.1 | 3.1 | 8 |
| | IM | 106.1 | 90.8 | 97.6 | 11.3 | 8 |

Table 4: Worst-case contingency for different operation strategies; IEEE-30 bus-10-node electrical–gas system.

| σ_{nm} | Centralized | Decentralized | Isolated |
|---------------|--------------|---------------|--------------|
| 1 | Line (12-13) | Line (12-13) | Line (12-13) |

| | | | |
|---|------------------------|------------------------|------------------------|
| 2 | Lines (12-13), (16-17) | Lines (12-13), (16-17) | Lines (12-13), (16-17) |
|---|------------------------|------------------------|------------------------|

4.2. Cascading contingency management with/without the DGFCs

To analyze the effect of the DGFCs on the cascading contingency management, the $n-1$ and $n-2$ security criteria with/without the DGFCs are taken into account. Tables 2 and 3 show the proposed cooperation problem results for $k=1$ and $k=2$, respectively. As Tables 1–3 show, with non- and single (double) contingent conditions, as anticipated, the operation costs of the PS and the NGS are increased. For example, as seen in Table 4, for $k=1$, i.e., an outage of the transmission line 13-12, results in the shutdown of the large thermal unit G2, based on Fig. 3, which is fully committed in the pre-contingency condition.

In this situation, the fast response GFUs, i.e., GFU-1 to GFU-3, should increase their output to compensate for the shortage of power generation. However, the generation dispatch of the GFUs is distributed, because most of the GFUs are located at the end of the NGS, with a gas supplier that is limited through the nodal gas pressure along the gas grid. There is often a drop in gas pressure at nodes 7 and 10, which causes a decrease in the gas flow to the loads. Another factor is that these GFUs are placed in the same nodes, with high-priority residential loads, i.e., L4 and L6. Therefore, the natural gas available to supply gas fuel for GFU-1 and GFU-3 can, at times, be substantially limited.

For the above reasons, the electrical and gas operation costs for single (double) contingency are increased. Tables 2 and 3 show the results for the electrical operation cost with the DGFCs. It is seen that the daily electrical operation costs for single and double contingency conditions are reduced with the DGFCs. This is mainly because the gas pressure is improved when the DGFCs are considered by the proposed cooperation problem. Further analysis has shown that with an increase in the number of contingencies in the PS, the unserved electrical and gas loads are increased. Interestingly, as can be seen from Tables 2 and 3 with the DGFCs, there is a lower increase in the unserved electrical and gas loads.

4.3. Comparison of three cooperation mechanisms

Here, three cooperation mechanisms, i.e., the centralized mechanism (CM), the decentralized mechanism (DM), and the isolated mechanism (IM), for the cooperation of the PS and the NGS are addressed in Tables 1–4. Note that in the IM, the decision-making in the PS and the NGS is carried out separately, i.e., the PS and the NGS are individually operated while preserving information for each energy system. In the CM there is a system operator for both energy systems, and thus, information can be exchanged without preserving information privacy. However, for the DM there are two system operators for each system, and thus, information can be exchanged

while preserving information privacy. Tables 1-4 provide the electrical and gas operation costs, the unserved electrical and gas loads, the number of cascade contingencies, and the calculation time. The tables show that the difference between the solution results obtained from the CM and the DM is negligible. Additionally, Tables 1–4 show that the values for the electrical operation cost, the gas operation costs, the unserved electrical and the gas loads for the IM are highest, while they are lowest for the CM. In the IM, the gas fuel supply of the GDUs is more curtailed by the NGS operator, and thus, these units are less dispatched by the PS operator. Moreover, their commitment results in a natural gas pressure drop in the residential gas load. On the other hand, these units are located in the same node as that of the residential gas loads, which has a higher supply priority. Thus, the gas fuel supply to the GFUs cannot be guaranteed once the IM is considered by both energy systems. In the same conditions, the CM and the DM by sharing information between two energy system operators can reduce the electrical and gas operation costs, as well as the unserved electrical and gas loads for both energy systems. However, in the CM, a consolidated system operator is considered, and consequently, the information privacy of both energy systems is not preserved. Thus, the DM has more advantages in the decision-making process when the information privacy of the separate energy systems is preserved in the collaborative operation of the PS and the NGS. Further analysis of Tables 1–4 shows that while the solution time in the proposed DM is higher than that of the other two methods, the solution time for the DM is still reasonable in terms of the hourly operation procedure.

4.4. Larger Integrated PS and NGS (Scalability analysis)

In this section, additional simulations are conducted on a modified IEEE 118-bus electricity system and 10-node gas system (which is named the IEEE 118-bus-10-node electrical–gas system) to evaluate the proposed optimization problem for a larger integrated PS and NGS and its robustness against different cascading contingencies. To illustrate the efficacy of the proposed optimization problem and method, results of a relatively larger test system are presented here to represent the computational times required for the proposed co-optimization model with and without the DGFCs and cooperation mechanisms versus the scale of the test systems. The modified IEEE-118 bus system has 54 thermal generators, including eight GFUs, 186 transmission lines, and 91 load buses. The total capacity of GFUs is 725 MW, which is 10% of the total generation capacity. The natural gas transmission comprises ten nodes and 10 pipelines. The gas load and electrical load profiles follow the same pattern as presented in Fig. 5. The test data for the IEEE 118-bus-10-node electrical–gas system are given at “motor.ece.iit.edu/data”. Further, the data of the IEEE 118-bus-10-node electrical–gas system can be found in “[Gas transsmion 118 10.xls](#)” at “motor.ece.iit.edu/data”. The proposed co-optimization model for this larger test

system is simulated in the same way as the previous test system. Tables 5 and 6 compare the operation results with (without) DGFCs for different cooperation mechanisms. The results of the tables are interesting in several ways:

(i) These tables show that the total operation cost with the DGFCs is reduced for different k s, i.e., $k = 0$ and $k = 5$, and cooperation mechanisms. Similar to the previous test system, as anticipated, the total operation electrical cost with the DGFCs is reduced as explained above. Furthermore, as mentioned, the gas and electrical unserved loads can be reduced by the DGFCs, and for this reason, the gas and electrical unserved loads for this larger test system model with DGFCs are also reduced.

(ii) The operation results obtained for $k = 0$ and $k = 3$ are consistent with those of the previous test system. For example, as can be seen from Tables 5 and 6, as expected, the total operation cost and the electrical and gas unserved loads of both systems for $k = 3$ are increased. An interesting point about the results in Table 6 is that the daily operation cost and the electrical and gas unserved loads for $k = 3$ are reduced with the DGFCs for the CM and DM.

(iii) The results obtained from three cooperation mechanisms, i.e., the CM, DM, and IM, for the cooperation of both the systems are summarized in these tables. Interestingly, the data in these tables are consistent with the results obtained in the previous case. For example, a negligible difference between the solution results obtained from the CM and the DM was evident. However, a significant difference between the solution results obtained from the IM and other cooperation mechanisms was detected.

(iv) It is noteworthy that the overall computation time of the CM and the DM is increased with the system size. Nevertheless, the computation times for the three cooperation mechanisms are acceptable, because our co-optimization problem is executed in the day-ahead timeframe, and the times are shorter than one hour. The most surprising aspect of the computation times is that the proposed DM provides a faster computation time than the other cooperation mechanisms, which validates the practicability of the proposed DM for larger test systems.

Table 5: Comparison of the operation results between different operation strategies; for $k = 0$; the IEEE-118 bus-10-node electrical-gas system.

| Method | | Total operation cost [M\$] | Gas unserved load [kcf] | Electrical unserved load [MWh] | Time [min] |
|------------------|----|-------------------------------|-------------------------------|--------------------------------------|---------------|
| Without DGFCs | DM | 1.811 | 0 | 0 | 28 |
| | CM | 1.810 | 0 | 0 | 43 |
| | IM | 1.843 | 0 | 0 | 21 |

| | | | | | |
|---------------|----|-------|---|---|----|
| With DGFCs | DM | 1.798 | 0 | 0 | 32 |
| | CM | 1.797 | 0 | 0 | 53 |
| | IM | 1.843 | 0 | 0 | 24 |

Table 6: Comparison of the operation results between different operation strategies; for $k = 3$; the IEEE-118 bus-10-node electrical-gas system.

| Method | | Total operation cost [M\$] | Gas unserved load [kcf] | Electrical unserved load [MWh] | Time [min] |
|------------------|----|-------------------------------|-------------------------------|--------------------------------------|---------------|
| Without DGFCs | DM | 2.101 | 91.1 | 567 | 32 |
| | CM | 2.112 | 92.1 | 564 | 54 |
| | IM | 2.315 | 123.2 | 878 | 25 |
| With DGFCs | DM | 1.961 | 85.3 | 297 | 37 |
| | CM | 1.962 | 84.1 | 289 | 62 |
| | IM | 2.315 | 124.6 | 778 | 27 |

5. Conclusions

This paper proposed a decentralized and hierarchical co-optimization mechanism for the collaborative cooperation of the PS and the NGS, which preserves both information privacy and the independence of decision-making for each energy system operator.

Firstly, a gas constraint model for gas flow transients in pipelines using dynamic gas flow constraints (DGFCs) was presented. Results from the implementation of the model on two test systems were compared with the results obtained from the steady-state constraints. Collectively, the case studies show that the application of steady-state and dynamic constraints of gas flows yields different results for the collaborative operation of both the PS and the NGS. Furthermore, the simulation results indicate that the inherent storage capability of the gas pipelines and the slower flow rate of gas flows, which causes the gas pressure to drop in some gas nodes of the NGS, would have been neglected through the steady-state gas flow model.

Secondly, this paper investigated cascading contingency management for the PS operator with DGFCs. It was found that in the context of the proposed cooperation problem, the use of DGFCs results in reclaiming operation results and better management of multi-contingencies.

Thirdly, a comparison was performed of simulation results pertaining to three different operation mechanisms, i.e., the centralized mechanism, the decentralized mechanism, and the isolated mechanism. The results show that the electrical and gas operation costs and the unserved electrical and gas loads for both energy systems have a

better performance by adopting the CM, although the results for the CM and the DM are very similar. The results suggest that the proposed DM can achieve efficient solution results while preserving decision-making independence and information privacy of individual energy systems.

Finally, the simulation results of the IEEE 118-bus-10-node electrical–gas system show that the proposed cooperation problem can be applied to large-scale test systems. Furthermore, the results obtained through a larger test system are consistent with those of the smaller test system. What is interesting about the data in this study is that the proposed DM can provide a faster computation time for a large-scale test system than the DM, which validates the practicability of the proposed DM for larger test systems.

Acknowledgment

The authors thank Dr. Hanna Niemelä for her assistance with proofreading the paper and for the editorial comments that greatly improved the manuscript.

REFERENCES

- [1] A. Alabdulwahab, A. Abusorrah, X. Zhang, and M. Shahidehpour, "Coordination of interdependent natural gas and electricity infrastructures for firming the variability of wind energy in stochastic day-ahead scheduling," *IEEE Transactions on Sustainable Energy*, vol. 6, no. 2, pp. 606-615, 2015.
- [2] A. Nikoobakht, J. Aghaei, M. Shafie-khah, and J. Catalão, "Continuous-Time Co-Operation of Integrated Electricity and Natural Gas Systems with Responsive Demands Under Wind Power Generation Uncertainty," *IEEE Transactions on Smart Grid*, 2020.
- [3] H. Jokar, B. Bahmani-Firouzi, M. Simab, "Bilevel model for security-constrained and reliability transmission and distribution substation energy management considering large-scale energy storage and demand side management," *Energy Reports, Vol. 8*, pp. 2617-2629, 2022.
- [4] A. Nikoobakht, J. Aghaei, and M. Mardaneh, "Securing highly penetrated wind energy systems using linearized transmission switching mechanism," *Applied Energy*, vol. 190, pp. 1207-1220, 2017.
- [5] R. A. Jabr, "Radial distribution load flow using conic programming," *IEEE transactions on power systems*, vol. 21, no. 3, pp. 1458-1459, 2006.
- [6] R. A. Jabr, "A conic quadratic format for the load flow equations of meshed networks," *IEEE Transactions on Power Systems*, vol. 22, no. 4, pp. 2285-2286, 2007.
- [7] B. Kocuk, S. S. Dey, and X. A. Sun, "New formulation and strong MISOCP relaxations for AC optimal transmission switching problem," *IEEE Transactions on Power Systems*, vol. 32, no. 6, pp. 4161-4170, 2017.

- [8] R. A. Jabr, "Optimal power flow using an extended conic quadratic formulation," *IEEE transactions on power systems*, vol. 23, no. 3, pp. 1000-1008, 2008.
- [9] C. Liu, M. Shahidehpour, Y. Fu, and Z. Li, "Security-constrained unit commitment with natural gas transmission constraints," *IEEE Trans. Power Syst*, vol. 24, no. 3, pp. 1523-1536, 2009.
- [10] A. Nikoobakht, J. Aghaei, H. Fallahzadeh-Abarghouei, and R. Hemmati, "Flexible Co-Scheduling of integrated electrical and gas energy networks under continuous and discrete uncertainties," *Energy*, vol. 182, pp. 201-210, 2019.
- [11] S. Badakhshan, M. Ehsan, M. Shahidehpour, N. Hajibandeh, M. Shafie-Khah, and J. P. Catalão, "Security-Constrained Unit Commitment With Natural Gas Pipeline Transient Constraints," *IEEE Transactions on Smart Grid*, vol. 11, no. 1, pp. 118-128, 2019.
- [12] C. Liu, M. Shahidehpour, and J. Wang, "Coordinated scheduling of electricity and natural gas infrastructures with a transient model for natural gas flow," *Chaos: An Interdisciplinary Journal of Nonlinear Science*, vol. 21, no. 2, p. 025102, 2011.
- [13] H. Khani and H. E. Z. Farag, "Optimal day-ahead scheduling of power-to-gas energy storage and gas load management in wholesale electricity and gas markets," *IEEE Transactions on Sustainable Energy*, vol. 9, no. 2, pp. 940-951, 2017.
- [14] A. Street, F. Oliveira, and J. M. Arroyo, "Contingency-constrained unit commitment with $n-k$ security criterion: A robust optimization approach," *IEEE Transactions on Power Systems*, vol. 26, no. 3, pp. 1581-1590, 2010.
- [15] A. Street, A. Moreira, and J. M. Arroyo, "Energy and reserve scheduling under a joint generation and transmission security criterion: An adjustable robust optimization approach," *IEEE transactions on Power Systems*, vol. 29, no. 1, pp. 3-14, 2013.
- [16] N. Romero, N. Xu, L. K. Nozick, I. Dobson, and D. Jones, "Investment planning for electric power systems under terrorist threat," *IEEE Transactions on Power Systems*, vol. 27, no. 1, pp. 108-116, 2011.
- [17] A. Moreira, A. Street, and J. M. Arroyo, "An adjustable robust optimization approach for contingency-constrained transmission expansion planning," *IEEE Transactions on Power Systems*, vol. 30, no. 4, pp. 2013-2022, 2014.
- [18] A. Ben-Tal and A. Nemirovski, *Lectures on modern convex optimization: analysis, algorithms, and engineering applications*. Siam, 2001.
- [19] A. J. Osiadacz and C. s. centre, "Simulation and analysis of gas networks," 1987.

- [20] S. Tosserams, L. Etman, P. Papalambros, and J. Rooda, "An augmented Lagrangian relaxation for analytical target cascading using the alternating direction method of multipliers," *Structural and multidisciplinary optimization*, vol. 31, no. 3, pp. 176-189, 2006.
- [21] Y. Ben-Haim, Info-gap decision theory: decisions under severe uncertainty. Academic Press, 2006. .
- [22] X. Wu and A. J. Conejo, "Security-constrained ACOPF: Incorporating worst contingencies and discrete controllers," *IEEE Transactions on Power Systems*, vol. 35, no. 3, pp. 1936-1945, 2019.
- [23] S. Dehghan, N. Amjady, and A. J. Conejo, "Adaptive robust transmission expansion planning using linear decision rules," *IEEE Transactions on Power Systems*, vol. 32, no. 5, pp. 4024-4034, 2017.
- [24] D. P. Bertsekas, Nonlinear Programming, 2nd ed. Belmont, MA, USA: Athena Scientific, 2003.
- [25] [Online]. Available: https://alroomi.org/multimedia/Power_Flow/30BusSystem/IEEE30BusSystemDATA2.pdf.